ARTICLE

Quantitative understanding of the initial stage of liquid to crystalline or amorphous phase transitions

Hao-De Dong,[1] Peng Zhang,[2] Ming-Yang Qin,[1] Jian Hui,[3] Hong Wang,[3,*] Zi-Kui Liu,[4,*] and X.-D. Xiang[1,2,5,*]

*Correspondence: hongwang2@sjtu.edu.cn (H. W.); liu@matse.psu.edu (Z. L.); xiangxd@sustech.edu.cn (X. X.)

Received: April 22, 2024; Accepted: August 7, 2024; Published Online: August 13, 2024; https://doi.org/10.59717/j.xinn-mater.2024.100086

GRAPHICAL ABSTRACT

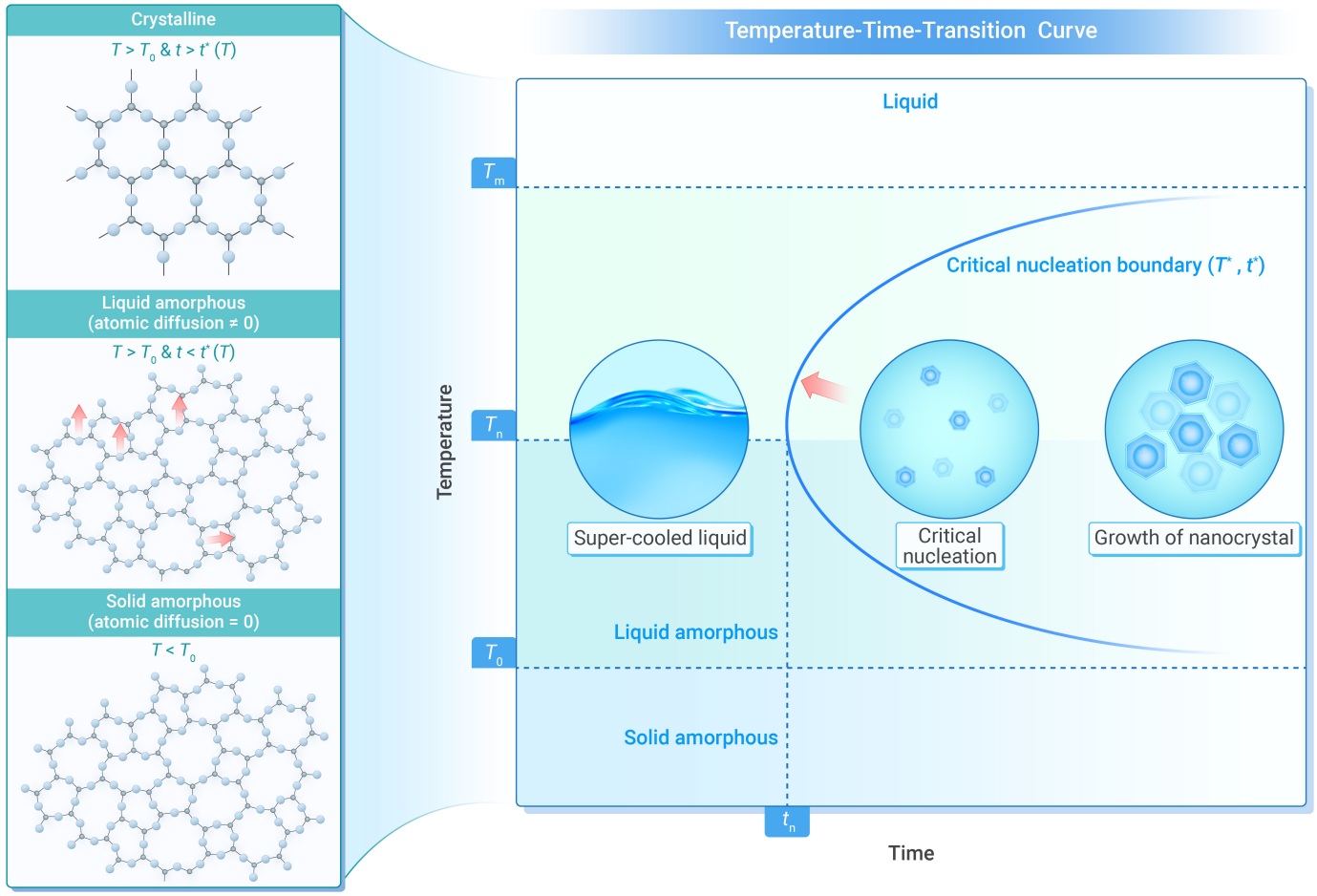

PUBLIC SUMMARY

- The time-temperature transition (TTT) curve is the critical boundary between the glass and crystal phases.
- Relating critical interface energy as a function of critical viscosity enables a quantitative model of TTT.
- The model reveals a new liquid to solid glass phase transition at T_0, and the nature of a glassy substance.

ARTICLE

www.the-innovation.org/materials

Quantitative understanding of the initial stage of liquid to crystalline or amorphous phase transitions

Hao-De Dong,[1] Peng Zhang,[2] Ming-Yang Qin,[1] Jian Hui,[3] Hong Wang,[3,*] Zi-Kui Liu,[4,*] and X.-D. Xiang[1,2,5,*]

[1]Department of Materials Science and Engineering, Southern University of Science and Technology, Shenzhen 518055, China

[2]Academy for Advanced Interdisciplinary Studies, Southern University of Science and Technology, Shenzhen 518055, China

[3]School of Materials Science and Engineering, Materials Genome Initiative Center & Zhangjiang Institute for Advanced Study, Shanghai Jiao Tong University, Shanghai 200240, China

[4]Department of Materials Science and Engineering, The Pennsylvania State University, University Park, PA 16802, USA

[5]Department of Physics, Southern University of Science and Technology, Shenzhen 518055, China

*Correspondence: hongwang2@sjtu.edu.cn (H. W.); liu@matse.psu.edu (Z. L.); xiangxd@sustech.edu.cn (X. X.)

Received: April 22, 2024; Accepted: August 7, 2024; Published Online: August 13, 2024; https://doi.org/10.59717/j.xinn-mater.2024.100086

Citation: Dong H., Zhang P., Qin M., et al., (2024). Quantitative understanding of the initial stage of liquid to crystalline or amorphous phase transitions. The Innovation Materials **2(3)**: 100086.

In 2005, Science magazine listed the "nature of a glassy substance" as one of the 125 most challenging scientific questions of the century. A quantitative understanding of the time-temperature transition (TTT) curve for critical nucleation of amorphous materials is crucial to answering this question. Despite extensive efforts over the past 70 years, a quantitative model for the TTT curve remains elusive due to a lack of understanding of physical properties such as the interfacial energy at the incubation time t^* for critical nucleation. In this study, a relationship between the critical nucleation viscosity and the interfacial energy as a function of t^* is established and a quantitative TTT model is developed. The model demonstrates excellent agreement with experimental TTT data for various amorphous materials. Most importantly, it allows the accurate and definitive determination of T_0, the true minimum crystallization temperature at the lower end-point of the TTT curve, as well as the temperature below which the amorphous liquid-to-solid state transition occurs. This offers an unambiguous answer to the nature of glassy substances: Above T_0, a liquid with constant amorphous structure relaxation; and below T_0, a solid with stable amorphous structure.

INTRODUCTION

The "nature of a glassy substance" was among the top 125 cutting-edge scientific questions proposed by Science magazine in 2005.[1] The debate centers on whether the amorphous state is liquid or solid in nature. Some researchers suggest that the system undergoes a transition from a supercooled liquid to a glassy state as the viscosity reaches 10^{12} or 10^{13} Pa·s.[2-4] Such a transition results in a loss of fluidity of the system, which behaves like a solid. Other researchers suggest that such a glassy state still belongs to a liquid state with an extremely slow relaxation rate, commonly supported by the observation of slow molecular flow in the window glass of medieval churches, even though its viscosity is well beyond 10^{13} Pa·s, resulting in a thin top and a thick bottom.[5-7]

The question then changes to whether there is a qualitative, rather than a quantitative, boundary separating amorphous into liquid and solid substances? Kauzmann and Gibbs et al. augured that, to avoid violating the third law of thermodynamics, the supercooled liquid state of any amorphous material should always undergo a liquid-to-solid transition above zero degrees Kelvin, named as the "Kauzmann temperature" T_K or the "ideal glass transition temperature" T_2.[5,8,9] However, Until now, T_K has been primarily conceptual, as it is difficult to determine or measure such a liquid-solid transition temperature.

In order to explain the "nature of a glassy substance", it is essential to develop a quantitative model to describe the transition from liquid to crystal/glass phase. Unfortunately, by far the majority of models have been limited to the qualitative level. A few quantitative models have not been sufficient to meet the experimental data.

MATERIALS AND METHODS

Construction of quantitative TTT curve model

As a fundamental element of the non-equilibrium phase diagram, the time-temperature transition (TTT) curve offers a valuable tool for understanding the phase transition in glass-forming systems. The curve corresponding to the initial of critical nucleation describes the condition of transition from a supercooled liquid to a crystalline state. Qualitatively, the transition boundary is defined by the lowest detectable volume fraction of crystalline phase, which is considered to be crystallinity at 10^{-6}.[10,11] The incubation time t^* required to reach this critical volume fraction varies significantly with the nucleation temperature T^* for a given material composition. On both the high and low temperature sides of the TTT curve, the nucleation incubation time approaches infinity. At or near the melting temperature (T_m), the system reversibly reaches an equilibrium state with fully equilibrated internal degrees of freedom. There is an intermediate temperature at which t^* is at its minimum, known as the "nose point" (T_n^*, t_n^*). Near the lower limit of the TTT curve, the internal degrees of freedom are not fully relaxed due to kinetic constraints, resulting in the system being trapped in a frozen state.

Turnbull and Uhlmann et al. developed a framework for the TTT curve in the 1950s and 1960s.[10,12-14] The framework is based on the Johnson-Mehl-Avrami theory, with t^* defined as a function of T^*:[15]

$$t^* = f(T^*) = \sqrt[4]{\frac{3x}{\pi I(T^*)\,u(T^*)^3}}, \tag{1}$$

where x is the volume fraction of crystallinity, $I(T^*)$ is the nucleation rate, and $u(T^*)$ the crystal growth rate. It is important to realize that all physical properties related to the TTT curve below T_m depend on both T and t. This is because for TTT curve line, denoted by (T^*,t^*), each T^* is associated with a specific value of t^* for a given material. The function describing t^* in terms of T^* is defined by Eq. (1), while its inverse function f^{-1} describes T^* in terms of t^*, i.e.:

$$T^* = f^{-1}(t^*). \tag{2}$$

Eq. (1) describes the incubation time t^* for the nucleation of a phase transition for different materials at different nucleation temperature T^*, which is a dynamic non-equilibrium process. The super-cooled liquids can be considered "in equilibrium states" with respect to small, local stochastic fluctuations, but "in non-equilibrium states" with respect to the phase transitions described by Eq. (1), which is the very nature of TTT diagrams.[16] The nucleation process, like any thermally activated processes, is both stochastic microscopically governed by thermal fluctuations and statistical mechanics, and deterministic macroscopically exemplified by master equations such as Eq. (1).[17]

The equations for $u(T^*)$ and $I(T^*)$ are as follows:[18-20]

$$u(T^*) = \frac{D_0}{\delta} e^{-\frac{\Delta G_C^d(T^*)}{k_B T^*}} \left(1 - e^{-\frac{V_m \Delta g_v(T^*)}{RT^*}}\right), \tag{3}$$

$$I(T^*) = \frac{D_0}{\delta^2} \frac{N_a}{V_m} e^{-\frac{\Delta G_C^d(T^*) + {}^n\Delta G_{heter}^*(T^*)}{k_B T^*}}, \tag{4}$$

where V_m is the molar volume, k_B the Boltzmann constant, R the gas constant, N_a the Avogadro number, D_0 the pre-factor for the diffusion coeffi-

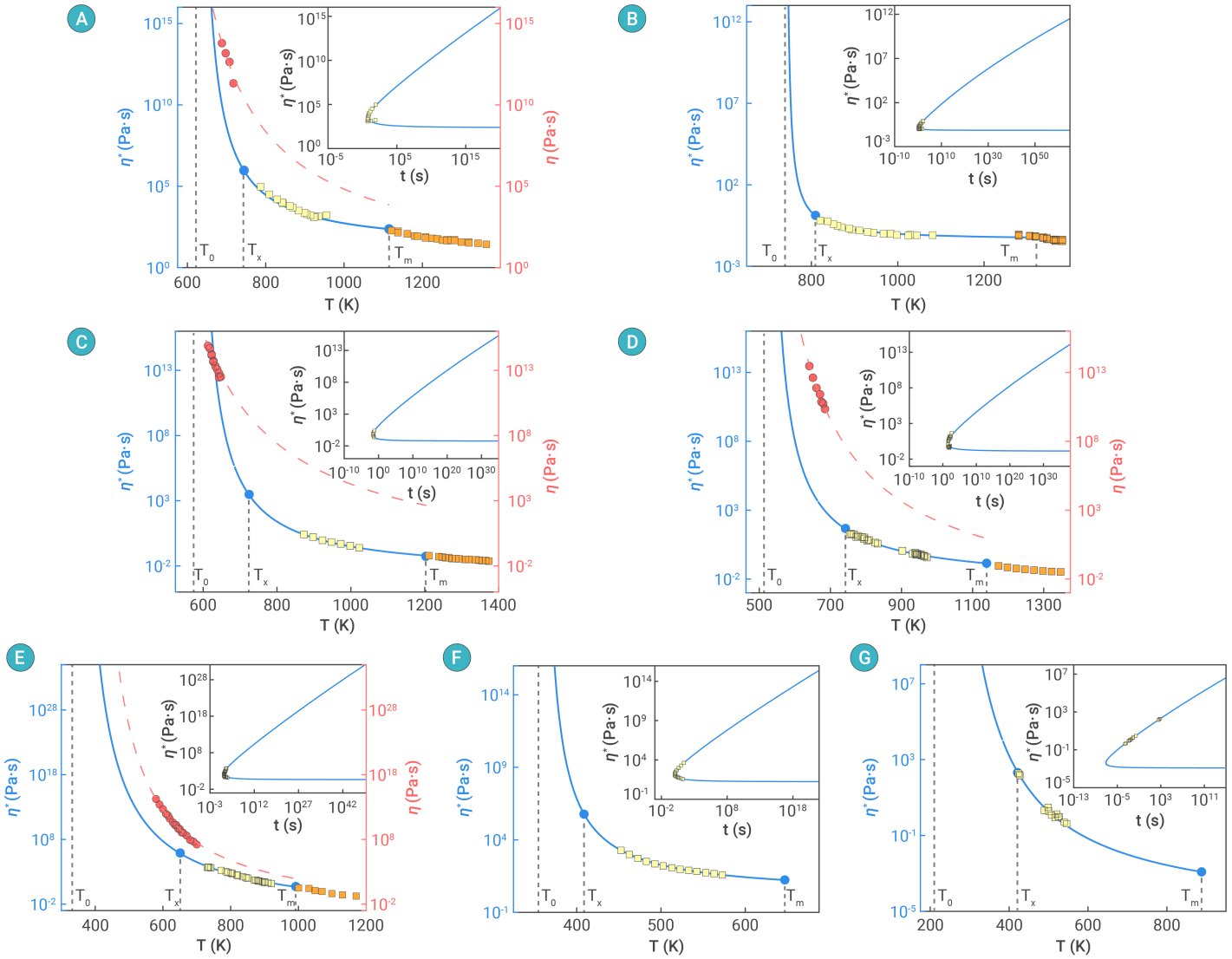

Figure 1. Temperature and time dependent curves of viscosity for amorphous alloys (A) $Zr_{57}Cu_{15.4}Ni_{12.6}Al_{10}Nb_5$, (B) $Zr_{55}Al_{22.5}Co_{22.5}$, (C) $Zr_{59.3}Cu_{28.8}Al_{10.4}Nb_{1.5}$, (D) $Zr_{58.5}Cu_{15.6}Ni_{12.8}Al_{10.3}Nb_{2.8}$, (E)$Zr_{41.2}Ti_{13.8}Cu_{12.5}Ni_{10}Be_{22.5}$, (F) $Au_{50}Cu_{25.5}Ag_{7.5}Si_{17}$, (G) $Ge_2Sb_2Te_5$. See text for details.

cient, which is proportional to $v\delta^2$, v the mean atomic jump frequency (10^{13}) and δ the mean atomic jump distance, $\Delta G_c^d(T^*)$ the atomic diffusion barrier from the liquid to the critical nuclei.

$\Delta g_v(T^*)$ represents the Gibbs energy per unit volume between the liquid and solid phases:[21]

$$g_v(T^*) = \frac{\Delta H_m}{V_m} - \frac{T^*}{T_m}\frac{\Delta H_m}{V_m} + \int_{T^*}^{T_m}\frac{\Delta C_p(T^*)}{V_m}dT - T^*\int_{T^*}^{T_m}\frac{\Delta C_p(T^*)}{T^* V_m}dT, \quad (5)$$

where ΔH_m is the molar enthalpy of melting, and ΔC_p the difference in heat capacity between the liquid and solid phases at constant pressure. It is important to note that although the latter two terms are of comparable magnitude to the first two terms over the temperature range from T_m to the minimum crystallization temperature, they are sometimes ignored in the literatures.[22-24]

"$\Delta G^*_{heter}(T^*)$ represents the critical energy barrier for heterogeneous nucleation of a nucleus:[25]

$$\Delta G^*_{heter}(T^*) = S(\theta)\Delta G^*_c(T^*) = S(\theta)\left(-\frac{16\pi\sigma(T^*)^3}{3\Delta g_v(T^*)}\right), \quad (6)$$

with

$$r^* = -\frac{2\sigma(T^*)}{\Delta g_v(T^*)} \quad (7)$$

where $\Delta G^*_c(T^*)$ is the critical energy barrier for homogeneous nucleation, r^* the critical nucleation radius, and σ the interfacial energy between the liquid and solid phases. The angular factor $S(\theta)$represents the difference in nucleation energy between the heterogeneous and homogeneous nucleation processes:[25]

$$S(\theta) = \frac{2 - 3\cos\theta + \cos^3\theta}{4}, \quad (8)$$

where θ is the wetting angle between the crystal nucleus and substrate.

The diffusion coefficient $D_n(T^*)$ can be determined using either the Arrhenius equation or the Stokes–Einstein equation as follows:[26,27]

$$D_n(T^*) = D_0 exp\left[-\frac{\Delta G_c^d(T^*)}{k_B T^*}\right] = \frac{k_B T^*}{3\pi\delta\eta(T^*)}, \quad (9)$$

where $\eta(T^*)$ is the critical nucleation viscosity of the super-cooled liquid. Thus, the energy barrier for diffusion at the critical condition $\Delta G_c^d(T^*)$ can be calculated using Eq. (9) as follows:

$$\Delta G_c^d(T^*) = k_B T^* ln\left[\frac{3\pi\delta D_0\eta(T^*)}{k_B T^*}\right]. \quad (10)$$

The VFT (Vogel-Fulcher-Tammann) equation is commonly used to describe the viscosity of a liquid as a function of temperature:[28]

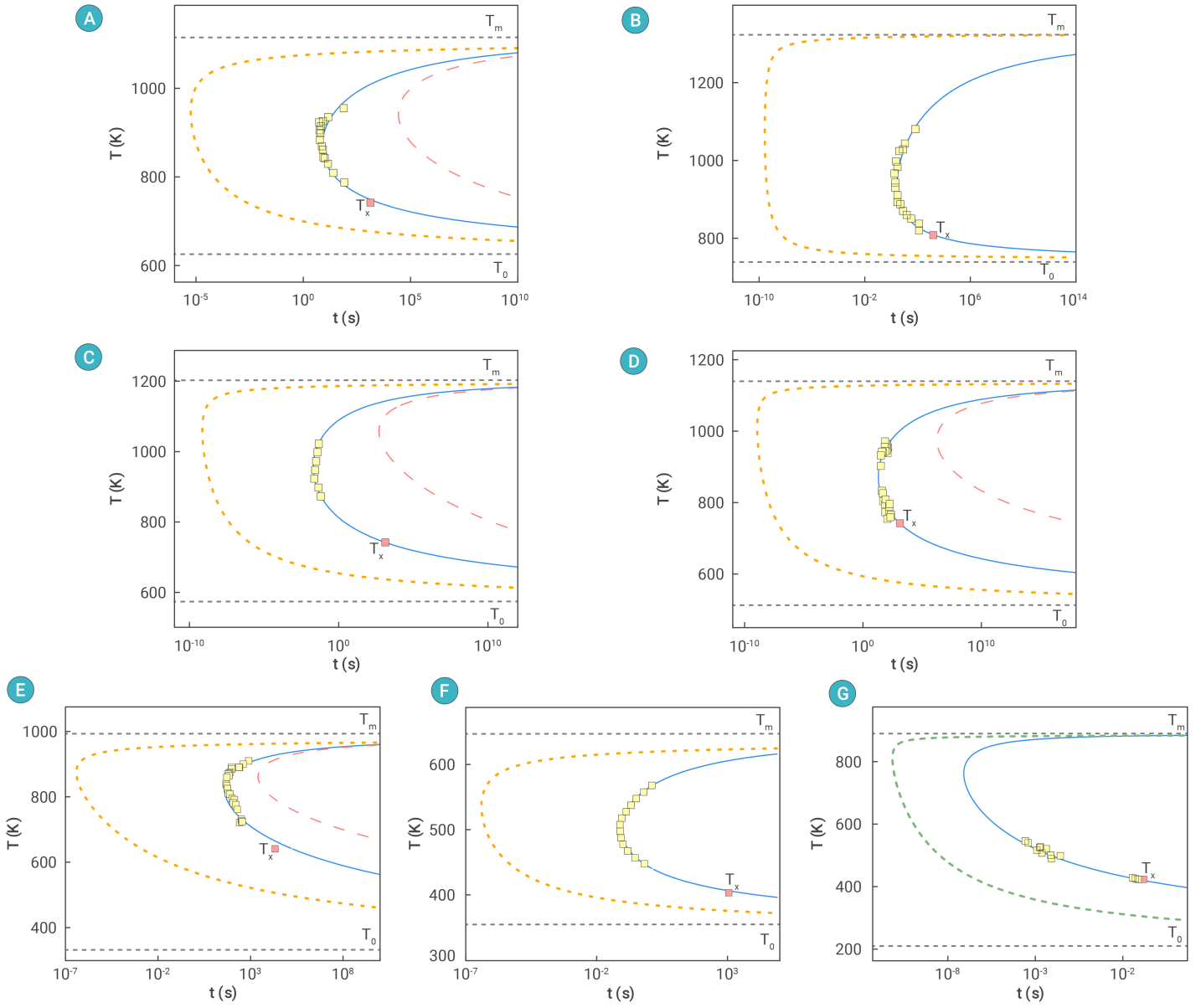

Figure 2. TTT curves for amophous alloys (A) $Zr_{57}Cu_{15.4}Ni_{12.6}Al_{10}Nb_5$, (B) $Zr_{55}Al_{22.5}Co_{22.5}$, (C) $Zr_{59.3}Cu_{28.8}Al_{10.4}Nb_{1.5}$, (D) $Zr_{58.5}Cu_{15.6}Ni_{12.8}Al_{10.3}Nb_{2.8}$, (E)$Zr_{41.2}Ti_{13.8}Cu_{12.5}Ni_{10}Be_{22.5}$, (F) $Au_{50}Cu_{25.5}Ag_{7.5}Si_{17}$, (G) $Ge_2Sb_2Te_5$. See text for details.

$$\eta(T) = \eta_0 exp\left(\frac{AT_0}{T - T_0}\right), \tag{11}$$

where η_0, A, and T_0 are typically unknown parameters and are commonly determined by fitting experimental values. The parameter η_0 represents the viscosity as the temperature approaches infinity, which cannot be measured experimentally. When the temperature is at or above T_m, the liquid is always in an equilibrium state and the viscosity at or above the melting point can be regarded as a time independent equilibrium parameter. Therefore, viscosity can be measured using various experiments that typically take seconds or longer, such as the Couette concentric cylinder viscometer, the rotating cup viscometer, or the container-less electrostatic levitation.[29-34] Using $\eta_{T_m} = \eta_0 \exp\left(\frac{AT_0}{T_m - T_0}\right)$, Eq. (11) can be rewritten as a new viscosity model that eliminates the parameter η_0:

$$\eta(T) = \eta_{T_m} exp\left(\frac{AT_0}{T_m - T_0}\frac{T_m - T}{T - T_0}\right), \tag{12}$$

It is crucial to realize that the VFT equation is only valid at temperatures above T_m, since below T_m the supercooled liquid undergoes a critical nucleation stage on different time scales. In other words, a single variable T-dependent VFT equation cannot describe the viscosity of a mixed state of supercooled liquid and crystalline. On conventional time scales where the viscosity of the liquid is measured, the materials are always in the crystalline state rather than the liquid state for $T_m > T > T_x$, where T_x is traditionally defined as the minimum crystallization temperature measured on a time scale of 100 s. This is exactly the reason why below T_m the TTT curve must be measured as a function of both T and t, rather than as a function of T alone. Reiner recognized this long before, and introduced a dimensionless parameter, the Deborah Number (DN) defined as the ratio of the relaxation time to the measurement/observation time, to describe the structural relaxation process of supercooled liquid.[35] The only way to describe viscosity as a single-valued function below T_m is to extend the VFT as a function of (T^*, t^*). Eq. (12) is then transformed accordingly as:

$$\eta^*(T^*) = \eta_{T_m} exp\left(\frac{AT_0}{T_m - T_0}\frac{T_m - T^*}{T^* - T_0}\right), \tag{13a}$$

where η^* is the viscosity at the critical nucleation stage. To determine A and T_0 in Eq. (13a), it is necessary to fit the experimental values of temperature T^*

at incubation time t^* to the TTT curve of critical nucleation. By replacing T^* in Eq. (13a) with Eq. (2), i.e. $T^* = f^{-1}(t^*)$, the quantitative relationship between $\eta^*$and t^* can be obtained:

$$\eta^*(t^*) = \eta_{T_m} \exp\left(\frac{AT_0}{T_m - T_0}\frac{T_m - f^{-1}(t^*)}{f^{-1}(t^*) - T_0}\right). \tag{13b}$$

Several theoretical models have been proposed in the literature to describe the solid-liquid interface energy with thermodynamic parameters. Uhlmann postulated that the critical nucleation energy barrier $\Delta G^*(T) = 50k_BT$ at $T = 0.8T_m$ (in accordance to the experimental values observed for most materials), and subsequently derived an empirical formula for the correlation between the solid-liquid interface energy σ and the melting enthalpy ΔH_m:[10]

$$\sigma^3 = \frac{0.192k_BT_m}{\pi}\frac{\Delta H_m^{\ 2}}{V_m^{\ 2}}. \tag{14}$$

However, the use of Eq. (14) results in a poor match with the TTT curve data, yielding t_n values that are several orders of magnitude different from the experimental values for our sample materials. This is demonstrated by the orange dotted lines in Figures 2A-G. Other interfacial energy models such as those presented in references, also incorporate both enthalpy and entropy of melting, but they also fail to achieve quantitative agreement with the experimental data.[22,36-38] Kalb et al. determined the solid-liquid interface energy of $Ge_2Sb_2Te_5$, a constant value, by measuring the maximum degree of supercooling.[39] Nevertheless, the calculated value of the TTT curve after numerical input still failed to match the experimental TTT data, as illustrated by the green dotted line in Figure 2G. The failure of these efforts underlines the necessary effort to use time dependent physical parameters to correctly describe a non-equilibrium phase transition process.

To obtain a more accurate expression for $\sigma(T^*)$, we analyze the critical balance of Eq. (3). We assume a small perturbation of all critical (C) nuclei with an increased radius of supercritical nuclei $(r^* + \delta)$, where δ is the diameter of the atom. Since the above assumption does not affect the number of nuclei per unit volume per unit time, the rates of critical and supercritical nucleation are equal. Therefore, the following relationship holds:

$$I_c(T^*) = \frac{D_0}{\delta^2}\frac{N_a}{V_m}e^{-\frac{\Delta G_c^d(T^*) + \Delta G_c^* S(\theta)}{k_BT^*}} = I_{sc}(T^*) = \frac{D_0}{\delta^2}\frac{N_a}{V_m}e^{-\frac{\Delta G_{sc}^d(T^*) + \Delta G_{sc}^* S(\theta)}{k_BT^*}}, \tag{15}$$

and this equation yields:

$$\Delta G_c^d(T^*) - \Delta G_{sc}^d(T^*) = (\Delta G_{sc}^* - \Delta G_c^*)S(\theta). \tag{16}$$

The term $(\Delta G_{sc}^* - \Delta G_c^*)$ can be defined as the total differential of ΔG^* with respect to T^* and r^*:

$$\Delta G_{sc}^* - \Delta G_c^* = \frac{\partial \Delta G_c^*}{\partial T^*}dT^* + \frac{\partial \Delta G_c^*}{\partial r^*}dr^*. \tag{17}$$

dT^* can be considered as the extra crystallization heat released from supercritical nuclear due to a small increase in δ. However, since the volume fraction of nuclei is extremely small $(x = 10^{-6})$, the temperature rise can be ignored $(dT^* = 0)$. Eq. (17) is simplified as follows:

$$\Delta G_{sc}^* - \Delta G_c^* = -2\pi\Delta g_v(T^*)r^{*2}\delta. \tag{18}$$

Since $\Delta G_c^d(T^*)$is significantly smaller than $\Delta G_c^* S(\theta)$, we must assume $\Delta G_{sc}^d(T^*) = 0$ to compensate for the increase in ΔG_{sc}^* shown by Eq. (18). Thus Eq. (16) can be simplified as follows:

$$\Delta G_c^d(T^*) \approx -2\pi\Delta g_v(T^*)r^{*2}\delta S(\theta). \tag{19}$$

From Eq. (20), it is possible to obtain the value of r^*:

$$r^* = \sqrt{-\frac{\Delta G_c^d(T^*)}{2\pi\delta S(\theta)\Delta g_v}}. \tag{20}$$

The interfacial energy $\sigma(T^*)$ for heterogeneous critical nucleation can be derived using Eq. (8):

$$\sigma(T^*) = \sqrt{-\frac{\Delta g_v(T^*)k_BT^* ln\left[\frac{3\pi\delta D_0\eta(T^*)}{k_BT^*}\right]}{8\pi\delta S(\theta)}}. \tag{21}$$

A one-to-one relationship is now established between the TTT curve (Eq. (1)) and the critical nucleation viscosity $\eta(T^*)$, which determines not only the diffusion coefficient (Eqs. (9 & 10)) but also the solid-liquid interfacial energy $\sigma(T^*)$ (Eq. (21)) through the nucleation rate (Eq. (4)) and the crystalline growth rate (Eq. (3)), from the supercooled liquid. In other words, the TTT curve (T^*, t^*), $\eta(T^*)$ and $\sigma(T^*)$ are interdependent, a measurement of one will determine the other two. Note that the critical nucleation viscosity $\eta(T^*)$, which determines the diffusion of atoms, is the driving force of nucleation, while $\sigma(T^*)$ is the critical nucleation barrier. Furthermore, the anchoring of viscosity to η_{T_m} at the melting point (Eq. (12)) connects the conventional VFT equation (Eq. (11)) valid above T_m and Eq. (13) valid below T_m. In other words, the conventional viscosity measurement above T_m can be used to validate Eq. (13) and to determine the critical viscosity below T_m. Only three material dependent fitting parameters $A, T_0$and $S(\theta)$ remain to be determined by a curve fitting process based on the experimental data of the TTT curve (T^*, t^*). The parameters A and T_0 in the critical nucleation viscosity model are intrinsic properties of the material system, while $S(\theta)$ is strongly influenced by the experimental conditions.

Experimental data analysis

There is a limited amount of experimental data on the TTT curve in amorphous systems. We found TTT curve data of only six alloy systems, $Zr_{57}Cu_{15.4}Ni_{12.6}Al_{10}Nb_5$, $Zr_{55}Al_{22.5}Co_{22.5}$, $Zr_{59.3}Cu_{28.8}Al_{10.4}Nb_{1.5}$, $Zr_{58.5}Cu_{15.6}Ni_{12.8}Al_{10.3}Nb_{2.8}$, $Zr_{41.2}Ti_{13.8}Cu_{12.5}$ $Ni_{10}Be_{22.5}$ and $Au_{50}Cu_{25.5}Ag_{7.5}Si_{17}$ with nose time $t_n^* > 10^{-2}$ s[29-34,40-43]. In addition, several reports have been published on the crystallization kinetics of a typical phase change material $Ge_2Sb_2Te_5$ $(t_n^* \sim 10^{-7}$ s).[44-50] However, we have only selected the experimental data from ref.[44], since it has the data with the widest range of time scales. The TTT curves for the first six amorphous alloys are derived from isothermal differential scanning calorimetry (DSC) experiments in the literature. Researchers extract the initial time of the crystallization peak as t^* for DSC curves at different constant temperatures T^* to obtain the TTT data set (T^*, t^*). The data for $Ge_2Sb_2Te_5$ were derived from heating calorimetric curves rather than isothermal calorimetric curves, which does not strictly conform to the definition of a TTT curve. However, due to the lack of experimental data on isothermal crystallization and the fact that most of the above data are far from the nose point of the TTT curve, we still regard them as TTT curve data. The data for each system include viscosity data, TTT curve data, and thermodynamic parameter data. Table 1 provides the thermodynamic parameters required for the calculation.

We have verified that the deviations in the value of x are negligible in all the above experimental conditions, i.e. the best fitting results are always obtained when the value of x is very close to 10^{-6}. Therefore, the default value of $x = 10^{-6}$ is always used in the fitting process.[10,11]

Experimental viscosity data at and above the melting point are extracted from the literature and are shown in the orange square in Figure 1, except for $Au_{50}Cu_{25.5}Ag_{7.5}Si_{17}$ and $Ge_2Sb_2Te_5$. Subsequently, the experimental TTT data (T^*, t^*) measured by isothermal DSC are also extracted from the literature. The blue lines are directly fitted to the data (yellow squares) using the TTT curve model Eq. (1) to determine the parameters: A, T_0 and $S(\theta)$ (listed in Table 2), with the help of Eqs. (3-10 & 21) for the critical nucleation viscosity η^* and interfacial energy$\sigma(T^*)$. The experimental TTT data (T^*, t^*) shown as yellow squares in both the main and inset figures of Figure 1 represent values of the critical nucleation viscosity determined from the (T^*, t^*) data according to Eqs. (13a-b). The same data (as red squares) determine not only the (T^*, t^*) curve shown as blue lines in Figure 2 with the help of Eq. (1), but also $\eta^*(T^*, t^*)$ with the help of Eq. (13) shown as blue lines in Figure 1. One can also obtain the values of $\sigma(T^*)$ with the help of Eq. (21) with the same values of (T^*, t^*), not shown in this paper.

The quantitative relationship between η^* and t^* (as shown in Eq. (13b)) is plotted in log-log form in the insets of Figure 1. Similar to the TTT curve, the $\eta^* - t^*$ curve is divided into an upper and a lower part. The lower part corre-

Table 1. Additional parameters from the literature necessary for the fitting process

Compounds	$\Delta H_m(10^3$ J/mol)	$V_m(10^{-6}$ m^3/mol)	T_m (K)	η_{T_m} (Pa·s)	ρ (g/cm^3)	δ(0.1 nm)	a^a	$b^a \times 10^{-3}$	$c^a \times 10^{-5}$	$d^a \times 10^6$
$Zr_{57}Cu_{15.4}Ni_{12.6}Al_{10}Nb_5$	9.4	11.78	1115	231	6.49	3.60	0	16.32 [51]	-0.83	6.32
$Zr_{55}Al_{22.5}Co_{22.5}$	7.67	11.07	1323	0.073	6.28	3.036	N/A	N/A	N/A	N/A
$Zr_{59.3}Cu_{28.8}Al_{10.4}Nb_{1.5}$	8.578	11.54	1203	0.062	6.64	3.32	0	-5.71 [52]	0.0605	10.31
$Zr_{58.5}Cu_{15.6}Ni_{12.8}Al_{10.3}Nb_{2.8}$	8.70	11.37	1140	0.139	6.70	3.00	0	12.80 [53]	-1.37	5.70
$Zr_{41.2}Ti_{13.8}Cu_{12.5}Ni_{10}Be_{22.5}$	8.2	10.032	993	4.559	5.984	3.34	95.28 [54]	-0.15	5.52	0
$Au_{50}Cu_{25.5}Ag_{7.5}Si_{17}$	5.844	9.48	647	16.886	13.45	3.10	33.67 [55]	-0.053	0	0
$Ge_2Sb_2Te_5$	14.373	19.03	888	N/A	5.995	2.68	N/A	N/A	N/A	N/A

a: The difference of heat capacity between the melt and solid is modeled by the following polynomial equation: $\Delta C_p = a + bT^* + cT^{*2} + dT^{*-2}$ J/(mol·K), with the constants a, b, c, d provided in the table.

Table 2. Parameters obtained by fitting

Compounds	A	T_0 (K)	θ(°)	$S(\theta)$
$Zr_{57}Cu_{15.4}Ni_{12.6}Al_{10}Nb_5$	2.16	621.97	46.59	0.0657
$Zr_{55}Al_{22.5}Co_{22.5}$	0.33	739.05	26.27	0.0077
$Zr_{59.3}Cu_{28.8}Al_{10.4}Nb_{1.5}$	3.69	574.21	31.34	0.0152
$Zr_{58.5}Cu_{15.6}Ni_{12.8}Al_{10.3}Nb_{2.8}$	4.04	513.19	27.77	0.0095
$Zr_{41.2}Ti_{13.8}Cu_{12.5}Ni_{10}Be_{22.5}$	22.06	332.22	40.95	0.0413
$Au_{50}Cu_{25.5}Ag_{7.5}Si_{17}$	1.96	354.67	47.51	0.0705
$Ge_2Sb_2Te_5$	18.87	206.54	35.15	0.0234

Table 3. Derived physical parameters obtained with quantitative knowledge of TTT curves

Compounds	R_C (K/s)	ΔG^*_C $(10^{-18}$J)	ΔG^*_{heter} $(10^{-19}$J)	r^* (nm)	σ (J/m^2)	ΔG^d_C $(10^{-19}$J)	D_n(m^2/s)	I(s^{-1}m^{-3})	u(m/s)
$Zr_{57}Cu_{15.4}Ni_{12.6}Al_{10}Nb_5$	31.5	10.05	6.60	2.83	0.299	2.52	1.01×10^{-15}	4.90×10^{8}	8.13×10^{-7}
$Zr_{55}Al_{22.5}Co_{22.5}$	138.6	151.56	11.72	7.94	0.574	1.34	2.62×10^{-11}	3.65×10^{-3}	1.61×10^{-2}
$Zr_{59.3}Cu_{28.8}Al_{10.4}Nb_{1.5}$	1.23×10^4	57.90	8.80	5.60	0.441	1.57	8.00×10^{-12}	4.99×10^{7}	4.92×10^{-3}
$Zr_{58.5}Cu_{15.6}Ni_{12.8}Al_{10.3}Nb_{2.8}$	13.4	113.73	10.88	6.57	0.628	1.55	2.47×10^{-12}	6.76×10^{-4}	2.04×10^{-3}
$Zr_{41.2}Ti_{13.8}Cu_{12.5}Ni_{10}Be_{22.5}$	4.0	20.42	8.43	4.15	0.283	2.03	2.33×10^{-14}	194.60	1.25×10^{-5}
$Au_{50}Cu_{25.5}Ag_{7.5}Si_{17}$	1.27×10^3	4.94	3.48	2.58	0.177	1.25	1.58×10^{-14}	2.56×10^{12}	1.35×10^{-5}
$Ge_2Sb_2Te_5$	1.9×10^9	**18.00**	3.91	4.54	0.208	**0.69**	9.89×10^{-10}	3.15×10^{22}	0.889

All parameters above are taken as values at T^*_n.

Table 4. Relevant parameters of two viscosity models

Compounds	conventional VFT equation			critical crystallization viscosity model		
	η_0(Pa·s)	A	T_0 (K)	η_{T_m}(Pa·s)	A	T_0 (K)
$Zr_{57}Cu_{15.4}Ni_{12.6}Al_{10}Nb_5$	0.529	11.24	511.05	15.10	2.16	621.97
$Zr_{55}Al_{22.5}Co_{22.5}$	N/A	N/A	N/A	4.83×10^{-2}	0.33	739.05
$Zr_{59.3}Cu_{28.8}Al_{10.4}Nb_{1.5}$	3.8×10^{-3}	26.29	369.70	2.13×10^{-3}	3.69	574.21
$Zr_{58.5}Cu_{15.6}Ni_{12.8}Al_{10.3}Nb_{2.8}$	4.83×10^{-5}	19.76	432.77	5.10×10^{-3}	4.04	513.19
$Zr_{41.2}Ti_{13.8}Cu_{12.5}Ni_{10}Be_{22.5}$	4.13×10^{-5}	24.64	368.10	6.94×10^{-5}	22.06	332.22
$Au_{50}Cu_{25.5}Ag_{7.5}Si_{17}$	N/A	N/A	N/A	1.57	1.96	354.67
$Ge_2Sb_2Te_5$	N/A	N/A	N/A	N/A	18.87	**206.54**

sponds to a higher temperature range where the critical nucleation viscosity does not change significantly with time and quickly reaches an equilibrium state. The upper part corresponds to a lower temperature range where the critical nucleation viscosity increases significantly on a time scale well

beyond millions of years. This indicates that the system is significantly affected by nucleation within the specified temperature range.

Figure 1 shows red dots representing low temperature viscosity data from the literatures with the exception of $Zr_{55}Al_{22.5}Co_{22.5}$, $Au_{50}Cu_{25.5}Ag_{7.5}Si_{17}$ and $Ge_2Sb_2Te_5$.[30,31,34] It should be noted that these values are taken without considering the constraint of critical nucleation conditions or corresponding time values. Using the traditional VFT equation (Eq. (11)) and the experimental viscosity results, we obtain the viscosity curves shown by the red dotted line in Figure 1. Subsequently, we calculate the TTT curves shown by the red dotted line in Figure 2 (except for $Zr_{55}Al_{22.5}Co_{22.5}$, $Au_{50}Cu_{25.5}Ag_{7.5}Si_{17}$ and $Ge_2Sb_2Te_5$.), with the theoretical TTT curve model including the traditional viscosity model and the interfacial energy model (i.e. Eqs. (1, 3-10, 11 & 21))) and these viscosity values, following traditional research procedures.[10,11] These lines differ significantly from the yellow square points of the experimental TTT data, highlighting the dual temperature and time dependent nature of the critical nucleation viscosity, and illustrating the importance of limiting (T, t) to the critical nucleation conditions of (T^*, t^*).

A number of physical parameters can be calculated by analyzing the TTT curve. Table 3 presents a set of derived physical parameters calculated at $T = T_n^*$.

DISCUSSION

Angell's analysis of Gibbs-Adam configurational entropy theory indicates that T_0 can be numerically equivalent to the Kauzmann temperature T_K, and further to the ideal glass transition temperature T_2.[56-58] The point T_0 determined by our model can be regarded as the critical point at which an amorphous liquid with finite viscosity and fluidity transitions to an amorphous solid with infinite viscosity, zero structural relaxation and fluidity. Moreover, the absence of collective phonons in the amorphous solid phase results in a lower entropy reduction with temperature decrease compared to the crystalline solid phase, thus resolving the Kauzmann paradox. The current study provides a reliable and accurate method to obtain T_0. Thus, between T_m and T_0 in $T-t$ space, the substance is always a liquid with time dependent viscosity over many orders of magnitude on the left of the TTT curve, and a crystalline solid on the right of the TTT curve; but below T_0, the substance becomes an amorphous solid state with time independent properties. This offers an unambiguous answer to the nature of glassy substances: above T_0, a liquid with constant amorphous structural relaxation; and below T_0, a solid with a stable amorphous structure.

The so called "minimal crystallization temperature", T_x, is typically determined by slow heating DSC experiments. T_x values for seven amorphous systems are extracted from the literature, shown as pink square dots in Figure 2. The slopes of the TTT curve remain large near T_x's, indicating that the system is still undergoing a non-equilibrium nucleation process. Therefore, the reported values of T_x are not the true minimum crystallization temperatures. As T^* approaches T_0, the critical nucleation viscosity approaches infinity according to Eq. (13a), causing $D_n(T^*)$ to become 0. Consequently, $I(T^*)$ and $u(T^*)$ also approach 0, corresponding to t^* approaching infinity. This indicates that T_0 is the lower end of the TTT curve, as shown in Figure 2. When the system is at a temperature above T_0, there is always a constant slow relaxation process, even though the nucleation incubation time is far beyond laboratory time scales of millions of years. Therefore, T_0 should be considered as the true minimum crystallization temperature. To this end, we realize that T_0 not only separates amorphous materials into liquid and solid substances, but also determines their possibility to crystallize or not. Above T_0, amorphous materials could always crystallize if we wait long enough, while below T_0, amorphous materials would never crystallize. Amorphous materials with lower T_0 usually have shorter t_n^*, faster R_c, less amorphous forming ability and lower stability.

As previously discussed, in the temperature range defined by the TTT curve, i.e. T_m to T_0, the conventional VFT equation with a single temperature variable is no longer applicable, as the system is in the critical crystallization stage of a non-equilibrium state. Specifically, in the temperature range from T_m to T_x, the crystallization incubation time scale is short, the "nose point" (T_n^*, t_n^*) of various materials ranges from 100s (as shown in this paper) to 10^{-12}s, and the degree of structural relaxation is high.[59] In the temperature range from T_x to T_0, the amorphous phase still demonstrates a slow fluidity and structural relaxation process, despite the dramatic increase in the crystallization incubation time over billions of years shown in the inset figures of Figure 1. As the incubation time is very long below T_x, conventional techniques can be used to measure viscosity without crystallization. However, researchers have demonstrated that these measurement data do not provide a smooth fit for the temperature range below T_x, as illustrated by the red dotted lines in Figure 1, and above T_m with one set of parameters.[30,31,60] In contrast, the critical nucleation viscosity model (Eq. (13a)) applied to the data below T_m and the VFT equation applied to the data above T_m enable the two sections of the viscosity-temperature curve to converge smoothly at the melting point with one set of parameters, as illustrated by the solid blue solid lines in Figure 1. The parameters of the above two cases for different material systems are summarized in Table 4 to show the difference.

Although the kinetics of crystallization is influenced by combined factors of physical parameters, the influence of T_0 is apparent. The significantly lower T_0 and 6-8 orders higher critical cooling rate R_c for $Ge_2Sb_2Te_5$ than for other alloy systems indicate an inverse correlation between R_c and T_0.

Melt quenching is a commonly used technique for preparing amorphous materials, in which the melt above the melting point undergoes a cooling process at a rate exceeding R_c, an effective quantitative indicator of glass forming ability (GFA).[10,61-63] Experimentally, R_c is usually obtained either indirectly by isothermal DSC or directly by continuous cooling DSC scanning. However, the resulting R_c is not a specific value, but rather a range, with a considerable degree of error. In this study, the quantified TTT curve can be used to derive the exact value of R_c, given in Table 3. Even in the absence of experimental data (T_n^*, t_n^*) for $Ge_2Sb_2Te_5$, the theoretical value of R_c can be obtained by fitting the theoretical value of the TTT curve over the entire temperature range.

As shown in Figure 2, it is feasible to produce multi-component amorphous films by annealing heterogeneous elemental multilayers at a given temperature $T = T^*$, where the critical nucleation viscosity is low enough for effective interlayer diffusion as long as the annealing time t is shorter than the corresponding incubation time t^*, to ensure mixing of the elements without formation of crystalline phases.[64] This low temperature amorphization technique has been used with subsequent heat treatment to achieve epitaxial thin film growth on single crystal substrates with variable compositions covering the entire phase diagram, known as combinatorial material chip technology.[65-75] For example, a calculation based on the diffusion coefficient D_n in Table 3 indicates that when the periodic thickness of the multilayer film is less than approximately 30 nm, the composition homogenization of $Au_{50}Cu_{25.5}Ag_{7.5}Si_{17}$ can be assured without crystallization before the annealing time reaches $t^*(T^* = 395\text{K}) = 5.9 \times 10^6$s.

Moreover, the quantification of the TTT curve enables the growth of nanocrystals in an amorphous matrix to be precisely regulated, thereby facilitating significant improvements in the mechanical properties and various physical and chemical properties of amorphous materials.[76-84] Different crystallinity sizes correspond to different non-critical TTT curves (with $x > 10^{-6}$). The intersection of the heating curve with a specific TTT at a specific temperature allows the material system to grow different sizes of nanocrystals in a controlled time scale. The critical nucleation radius, as presented in Table 3, is a key parameter in the operational framework of this technique, which serves to constrain the minimum size of the precipitated nanocrystalline phase.

The phase change memory device is capable of realizing the reversible transformation of amorphous (high resistivity, low reflectance) and crystalline (low resistivity, high reflectance) phases through the application of a laser or electrical pulse, which enables the storage of data 1 and 0.[85] The quantitative acquisition and analysis of TTT curves plays an important role in guiding the optimization process of phase-change memory materials.[86] Phase change memory materials in this application are expected to demonstrate high phase thermal stability and to maintain a metastable amorphous state at operating temperature for an extended period of time. Since T_0 for $Ge_2Sb_2Te_5$ is 206 K, the material is in the liquid state at operating temperature. However, the critical nucleation viscosity of $Ge_2Sb_2Te_5$ at room temperature is of the order of 10^{12} Pa·s, which corresponds to a crystallization incubation time of 10^{33} s (or 10^{24} years), as shown in the inset plot of Figure 1G. This suggests that the $Ge_2Sb_2Te_5$ based phase change memory device

exhibits sufficient stability in the amorphous state before crystallization. Phase change materials in this application are also expected to demonstrate a rapid transition rate between the crystalline and amorphous states to enhance the efficiency of the phase change memory device. Figure 2G illustrates that the TTT curve nose point time of $Ge_2Sb_2Te_5$ reaches the time scale of 10^{-7}s. Further reduction of this time scale would require quantitative TTT information on other optimization materials.

CONCLUSION

In summary, this study presents a quantitative model that relates the interfacial energy and critical nucleation viscosity for the super-cooled liquid phase, which depend on the nucleation temperature and incubation time (T^*,t^*) in connection with quantitative TTT curves through Eqs. (1, (13a-b & 21). The study successfully obtains TTT curves for seven bulk metallic glasses (BMG), which are in good agreement with time dependent measurements reported in the literatures. This model provides crucial insights into the quantitative description of the dynamic nucleation and growth of crystalline phases. In addition, this method allows a precise and unambiguous determination of T_0, the lower end-point of the TTT curve and the true minimum crystallization temperature, as well as the temperature at which the liquid-to-solid transition of the amorphous state occurs. This new model provides a new perspective on the "nature of a glassy substance".[1,2,87–89] As the T_n^* values in the TTT curves can span more than 10 orders of magnitude for different materials, with the shortest being on the sub-picosecond scale, future experimental techniques should be revolutionized to overcome the measurement barrier.

REFERENCES

1. So much more to know. (2005). Science **309**: 78-102. DOI: 10.1126/science.309.5731.78b.
2. Debenedetti, P.G. and Stillinger, F.H. (2001). Supercooled liquids and the glass transition. Nature **410**: 259–267. DOI: 10.1038/35065704.
3. Gao, Q. and Jian, Z. (2020). Predicting the thermodynamic ideal glass transition temperature in glass-forming liquids. Materials **13**: 2151. DOI: 10.3390/ma13092151.
4. Kawazoe, Y., Yu, J.-Z., Tsai, A.-P., et al. (1997). Phase diagrams and physical properties of nonequilibrium alloys. Subvol. A. (ed). Nonequilibrium phase diagrams of ternary amorphous alloys (Springer).
5. Kauzmann, W. (1948). The nature of the glassy state and the behavior of liquids at low temperatures. Chem. Rev. **43**: 219–256. DOI: 10.1021/cr60135a002.
6. Fellers, W.O. (1990). Materials science, testing, and properties for technicians (Prentice Hall).
7. Zhang, K., Zhang, Z., Pan, H., et al. (2024). Taming heat with tiny pressure. The Innovation **5**: 100577. DOI: 10.1016/j.xinn.2024.100577.
8. Welch, R.S., Zanotto, E.D., Wilkinson, C.J., et al. (2023). Cracking the kauzmann paradox. Acta Mater. **254**: 118994. DOI: 10.1016/j.actamat.2023.118994.
9. Gibbs, J.H. and DiMarzio, E.A. (1958). Nature of the glass transition and the glassy state. J. Chem. Phys. **28**: 373–383. DOI: 10.1063/1.1744141.
10. Uhlmann, D.R. (1972). A kinetic treatment of glass formation. J. Non-Cryst. Solids **7**: 337–348. DOI: 10.1016/0022-3093(72)90269-4.
11. Uhlmann, D.R. (1977). Glass formation. J. Non-Cryst. Solids **25**: 42–85. DOI: 10.1016/0022-3093(77)90090-4.
12. Turnbull, D. and Cohen, M.H. (2004). Concerning reconstructive transformation and formation of glass. J. Chem. Phys. **29**: 1049–1054. DOI: 10.1063/1.1744654.
13. Cohen, M.H. and Turnbull, D. (2004). Molecular transport in liquids and glasses. J. Chem. Phys. **31**: 1164–1169. DOI: 10.1063/1.1730566.
14. Davies, H.A. and Lewis, B.G. (1976). Metallic glasses and the avoidance of crystallization in metallic melts. Faraday Discuss. Chem. Soc. **61**: 100–109. DOI: 10.1039/DC9766100100.
15. Barmak, K. (2010). A commentary on: "Reaction kinetics in processes of nucleation and growth"*. Metall. Mater. Trans. A **41**: 2711–2775. DOI: 10.1007/s11661-010-0421-1.
16. Kelton, K.F. and Greer, A.L. (2010). Chapter 2 - The classical theory. Kelton, K.F. and Greer, A.L. (eds). Pergamon materials series (Pergamon), pp: 19-54. DOI: 10.1016/S1470-1804(09)01502-8.
17. Liu, Z.-K. (2023). Thermodynamics and its prediction and calphad modeling: Review, state of the art, and perspectives. Calphad **82**: 102580. DOI: 10.1016/j.calphad.2023.102580.
18. Turnbull, D. (1962). On the relation between crystallization rate and liquid structure. J. Phys. Chem. **66**: 609–613. DOI: 10.1021/j100810a009.
19. Turnbull, D. and Fisher, J.C. (1949). Rate of nucleation in condensed systems. J. Chem. Phys. **17**: 71–73. DOI: 10.1063/1.1747055.
20. Liu, F., Chen, K., and Xue, D. (2023). How to fast grow large-size crystals. The Innovation **4**: 100458. DOI: 10.1016/j.xinn.2023.100458.
21. Zanotto, E.D. and James, P.F. (1985). Experimental tests of the classical nucleation theory for glasses. J. Non-Cryst. Solids **74**: 373–394. DOI: 10.1016/0022-3093(85)90080-8.
22. Turnbull, D. (1950). Formation of crystal nuclei in liquid metals. J. Appl. Phys. **21**: 1022–1028. DOI: 10.1063/1.1699435.
23. Hoffman, J.D. (1958). Thermodynamic driving force in nucleation and growth processes. J. Chem. Phys. **29**: 1192–1193. DOI: 10.1063/1.1744688.
24. Thompson, C.V. and Spaepen, F. (1979). On the approximation of the free energy change on crystallization. Acta Metall. **27**: 1855–1859. DOI: 10.1016/0001-6160(79)90076-2.
25. Porter, D.A., Easterling, K.E., and Sherif, M.Y. (2009). Phase transformations in metals and alloys (revised reprint) (CRC Press).
26. Krynicki, K., Green, C.D., and Sawyer, D.W. (1978). Pressure and temperature dependence of self-diffusion in water. Faraday Discuss. Chem. Soc. **66**: 199–208. DOI: 10.1039/DC9786600199.
27. Einstein, A. (1905). On the motion of small particles suspended in liquids at rest required by the molecular-kinetic theory of heat. Ann. Phys. **17**: 208. DOI: 10.1002/andp.19053220806.
28. Garca-Coln, L.S., del Castillo, L.F., and Goldstein, P. (1989). Theoretical basis for the vogel-fulcher-tammann equation. Phys. Rev. B **40**: 7040–7044. DOI: 10.1103/PhysRevB.40.7040.
29. Waniuk, T.A., Busch, R., Masuhr, A., et al. (1998). Equilibrium viscosity of the $Zr_{41.2}Ti_{13.8}Cu_{12.5}Ni_{10}Be_{22.5}$ bulk metallic glass-forming liquid and viscous flow during relaxation, phase separation, and primary crystallization. Acta Mater. **46**: 5229-5236. DOI: 10.1016/S1359-6454(98)00242-0.
30. Hembree, W. (2015). High temperature rheology of Zr-based bulk metallic glass forming liquids. PhD thesis. (Saarland University).
31. Evenson, Z., Raedersdorf, S., Gallino, I., et al. (2010). Equilibrium viscosity of Zr–Cu–Ni–Al–Nb bulk metallic glasses. Scr. Mater. **63**: 573–576. DOI: 10.1016/j.scriptamat.2010.06.008.
32. Mukherjee, S., Kang, H.-G., Johnson, W., et al. (2004). Noncontact measurement of crystallization behavior, specific volume, and viscosity of bulk glass-forming Zr-Al-Co-(Cu) alloys. Phys. Rev. B **70**: 174205. DOI: 10.1103/PhysRevB.70.174205.
33. Mukherjee, S., Schroers, J., Zhou, Z., et al. (2004). Viscosity and specific volume of bulk metallic glass-forming alloys and their correlation with glass forming ability. Acta Mater. **52**: 3689–3695. DOI: 10.1016/j.actamat.2004.04.023.
34. Bai, F.X., Yao, J.H., Wang, Y.X., et al. (2017). Crystallization kinetics of an Au-based metallic glass upon ultrafast heating and cooling. Scr. Mater. **132**: 58–62. DOI: 10.1016/j.scriptamat.2017.02.001.
35. Reiner, M. (1964). The deborah number. Phys. Today **17**: 62–62. DOI: 10.1063/1.3051374.
36. Miedema, A.R. and Broeder, F.J.A.d. (1979). On the interfacial energy in solid-liquid and solid-solid metal combinations. Int. J. Mater. Res. **70**: 14–20. DOI: 10.1515/ijmr-1979-700103.
37. Boer, F.R.d., Mattens, W.C.M., Boom, R., et al. (1988). Cohesion in metals. Transition metal alloys (Amsterdam, Netherlands; North-Holland;).
38. Benedictus, R., Böttger, A., and Mittemeijer, E. (1996). Thermodynamic model for solid-state amorphization in binary systems at interfaces and grain boundaries. Phys. Rev. B **54**: 9109. DOI: 10.1103/PhysRevB.54.9109.
39. Kalb, J.A., Spaepen, F., and Wuttig, M. (2005). Kinetics of crystal nucleation in undercooled droplets of sb- and te-based alloys used for phase change recording. J. Appl. Phys. **98**: 054910. DOI: 10.1063/1.2037870.
40. Mukherjee, S., Zhou, Z., Schroers, J., et al. (2004). Overheating threshold and its effect on time–temperature-transformation diagrams of zirconium based bulk metallic glasses. Appl. Phys. Lett. **84**: 5010–5012. DOI: 10.1063/1.1763219.
41. Ericsson, A., Pacheco, V., Sahlberg, M., et al. (2020). Transient nucleation in selective laser melting of Zr-based bulk metallic glass. Mater. Des. **195**: 108958. DOI: 10.1016/j.matdes.2020.108958.
42. Hays, C.C., Schroers, J., Johnson, W.L., et al. (2001). Vitrification and determination of the crystallization time scales of the bulk-metallic-glass-forming liquid $Zr_{58.5}Nb_{2.8}Cu_{15.6}Ni_{12.8}Al_{10.3}$. Appl. Phys. Lett. **79**: 1605-1607. DOI: 10.1063/1.1398605.
43. Kim, Y.J., Busch, R., Johnson, W.L., et al. (1996). Experimental determination of a time–temperature - transformation diagram of the undercooled $Zr_{41.2}Ti_{13.8}Cu_{12.5}Ni_{10.0}Be_{22.5}$ alloy using the containerless electrostatic levitation processing technique. Appl. Phys. Lett. **68**: 1057-1059. DOI: 10.1063/1.116247.
44. Zhao, J., Hui, J., Ye, Z., et al. (2022). Exploring "no man's land"—arrhenius crystallization of thin-film phase change material at 1 000 000 k s^{-1} via nanocalorimetry. Adv. Mater. Interfaces **9**: 2200429. DOI: 10.1002/admi.202200429.
45. Orava, J., Greer, A.L., Gholipour, B., et al. (2012). Characterization of supercooled liquid $Ge_2Sb_2Te_5$ and its crystallization by ultrafast-heating calorimetry. Nat. Mater. **11**: 279–283. DOI: 10.1038/nmat3275.
46. Chen, B., ten Brink, G.H., Palasantzas, G., et al. (2017). Crystallization kinetics of gesbte phase-change nanoparticles resolved by ultrafast calorimetry. J. Phys. Chem. C **121**: 8569–8578. DOI: 10.1021/acs.jpcc.6b11707.
47. Gourvest, E., Pelissier, B., Vallée, C., et al. (2012). Impact of oxidation on $Ge_2Sb_2Te_5$ and gete phase-change properties. J. Electrochem. Soc. **159**: H373. DOI: 10.1149/2.027204jes.
48. Nozard, H. and Schiettekatte, F. (2021). Arrhenius behavior of crystallization at up to

184 000 k/s in $Ge_2Sb_2Te_5$ thin films. AIP Adv. **11**: 085226. DOI: 10.1063/5.0058586.
49. Jeyasingh, R., Fong, S.W., Lee, J., et al. (2014). Ultrafast characterization of phase-change material crystallization properties in the melt-quenched amorphous phase. Nano Lett. **14**: 3419–3426. DOI: 10.1021/nl500940z.
50. Pries, J., Wei, S., Wuttig, M., et al. (2019). Switching between crystallization from the glassy and the undercooled liquid phase in phase change material $Ge_2Sb_2Te_5$. Adv. Mater. **31**: 1900784. DOI: 10.1002/adma.201900784.
51. Glade, S.C., Busch, R., Lee, D.S., et al. (2000). Thermodynamics of $Cu_{47}Ti_{34}Zr_{11}Ni_8$, $Zr_{52.5}Cu_{17.9}Ni_{14.6}Al_{10}Ti_5$ and $Zr_{57}Cu_{15.4}Ni_{12.6}Al_{10}Nb_5$ bulk metallic glass forming alloys. J. Appl. Phys. **87**: 7242-7248. DOI: 10.1063/1.372975.
52. Heinrich, J., Busch, R., and Nonnenmacher, B. (2012). Processing of a bulk metallic glass forming alloy based on industrial grade Zr. Intermetallics **25**: 1–4. DOI: 10.1016/j.intermet.2012.02.011.
53. Gallino, I., Shah, M.B., and Busch, R. (2007). Enthalpy relaxation and its relation to the thermodynamics and crystallization of the $Zr_{58.5}Cu_{15.6}Ni_{12.8}Al_{10.3}Nb_{2.8}$ bulk metallic glass-forming alloy. Acta Mater. **55**: 1367-1376. DOI: 10.1016/j.actamat.2006.09.040.
54. Busch, R., Kim, Y.J., and Johnson, W.L. (1995). Thermodynamics and kinetics of the undercooled liquid and the glass transition of the $Zr_{41.2}Ti_{13.8}Cu_{12.5}Ni_{10.0}Be_{22.5}$ alloy. J. Appl. Phys. **77**: 4039-4043. DOI: 10.1063/1.359485.
55. Bünz, J. and Wilde, G. (2013). Direct measurement of the kinetics of volume and enthalpy relaxation of an Au-based bulk metallic glass. J. Appl. Phys. **114**: 223503. DOI: 10.1063/1.4843716.
56. Angell, C.A. (1997). Entropy and fragility in supercooling liquids. J. Res. Natl. Inst. Stand. Technol. **102**: 171–185. DOI: 10.6028/jres.102.013.
57. Tatsumisago, M., Halfpap, B.L., Green, J.L., et al. (1990). Fragility of Ge-As-Se glass-forming liquids in relation to rigidity percolation, and the kauzmann paradox. Phys. Rev. Lett. **64**: 1549–1552. DOI: 10.1103/PhysRevLett.64.1549.
58. Abiad, M.G., Carvajal, M.T., and Campanella, O.H. (2009). A review on methods and theories to describe the glass transition phenomenon: Applications in food and pharmaceutical products. Food Eng. Rev. **1**: 105–132. DOI: 10.1007/s12393-009-9009-1.
59. Zhong, L., Wang, J., Sheng, H., et al. (2014). Formation of monatomic metallic glasses through ultrafast liquid quenching. Nature **512**: 177–180. DOI: 10.1038/nature13617.
60. Evenson, Z., Schmitt, T., Nicola, M., et al. (2012). High temperature melt viscosity and fragile to strong transition in Zr–Cu–Ni–Al–Nb(Ti) and $Cu_{47}Ti_{34}Zr_{11}Ni_8$ bulk metallic glasses. Acta Mater. **60**: 4712–4719. DOI: 10.1016/j.actamat.2012.05.019.
61. Klement, W., Willens, R.H., and Duwez, P.O.L. (1960). Non-crystalline structure in solidified gold–silicon alloys. Nature **187**: 869–870. DOI: 10.1038/187869b0.
62. Lu, Z.P. and Liu, C.T. (2002). A new glass-forming ability criterion for bulk metallic glasses. Acta Mater. **50**: 3501–3512. DOI: 10.1016/S1359-6454(02)00166-0.
63. Lu, Z.P., Bei, H., and Liu, C.T. (2007). Recent progress in quantifying glass-forming ability of bulk metallic glasses. Intermetallics **15**: 618–624. DOI: 10.1016/j.intermet.2006.10.017.
64. Schwarz, R.B. and Johnson, W.L. (1983). Formation of an amorphous alloy by solid-state reaction of the pure polycrystalline metals. Phys. Rev. Lett. **51**: 415–418. DOI: 10.1103/PhysRevLett.51.415.
65. Chang, H., Takeuchi, I., and Xiang, X.-D. (1999). A low-loss composition region identified from a thin-film composition spread of $(Ba_{1-x-y}Sr_xCa_y)TiO_3$. Appl. Phys. Lett. **74**: 1165–1167. DOI: 10.1063/1.123475.
66. Takeuchi, I., Chang, H., Gao, C., et al. (1998). Combinatorial synthesis and evaluation of epitaxial ferroelectric device libraries. Appl. Phys. Lett. **73**: 894–896. DOI: 10.1063/1.122030.
67. Wang, J., Yoo, Y., Gao, C., et al. (1998). Identification of a blue photoluminescent composite material from a combinatorial library. Science **279**: 1712–1714. DOI: DOI: 10.1126/science.279.5357.1712.
68. Xiang, X.D. (1998). Combinatorial synthesis and high throughput evaluation of functional oxides-a integrated materials chip approach. Mater. Sci. Eng. B **56**: 246–250. DOI: 10.1016/S0921-5107(98)00221-9.
69. Schultz, P.G. and Xiang, X.-D. (1998). Combinatorial approaches to materials science. Curr. Opin. Solid State Mater. Sci. **3**: 153–158. DOI: 10.1016/S1359-0286(98)80081-8.
70. Xiang, X.D. (1998). Combinatorial synthesis and high throughput evaluation of functional materials: An integrated materials chip approach to discovery, optimization and study of advanced materials. Mater. Today **1**: 23–26. DOI: 10.1016/S1369-7021(98)80009-6.
71. Xiang, X.-D. (1999). Combinatorial materials synthesis and high-throughput screening: An integrated materials chip approach to mapping phase diagrams and discovery and optimization of functional materials. Biotechnology and Bioengineering **61**: 227–241. DOI: 10.1002/(SICI)1097-0290(1998)61:4<227::AID-CC5>3.0.CO;2-F.
72. Xiang, X.-D. (1999). Combinatorial materials synthesis and screening: An integrated materials chip approach to discovery and optimization of functional materials. Annu. Rev. Mater. Res. **29**: 149–171. DOI: 10.1146/annurev.matsci.29.1.149.
73. Yoo, Y.-K., Duewer, F., Yang, H., et al. (2000). Room-temperature electronic phase transitions in the continuous phase diagrams of perovskite manganites. Nature **406**: 704–708. DOI: 10.1038/35021018.
74. Li, J., Duewer, F., Gao, C., et al. (2000). Electro-optic measurements of the ferroelectric-paraelectric boundary in $Ba_{1-x}Sr_xTiO_3$ materials chips. Appl. Phys. Lett. **76**: 769–771. DOI: 10.1063/1.125889.
75. Fister, L. and Johnson, D.C. (1992). Controlling solid-state reaction mechanisms using diffusion length in ultrathin-film superlattice composites. J. Am. Chem. Soc. **114**: 4639–4644. DOI: 10.1021/ja00038a029.
76. Abrosimova, G.E., Matveev, D.V., and Aronin, A.S. (2022). Nanocrystal formation in homogeneous and heterogeneous amorphous phases. Phys.-Usp. **65**: 227–244. DOI: 10.3367/UFNe.2021.04.038974.
77. Andrievski, R.A. and Glezer, A.M. (2009). Strength of nanostructures. Phys.-Usp. **52**: 315–334. DOI: 10.3367/UFNe.0179.200904a.0337.
78. Greer, A.L. (2001). Partially or fully devitrified alloys for mechanical properties. Mater. Sci. Eng. A **304–306**: 68–72. DOI: 10.1016/S0921-5093(00)01449-0.
79. Sun, L.G., Wu, G., Wang, Q., et al. (2020). Nanostructural metallic materials: Structures and mechanical properties. Mater. Today **38**: 114–135. DOI: 10.1016/j.mattod.2020.04.005.
80. Kou, H., Lu, J., and Li, Y. (2014). High-strength and high-ductility nanostructured and amorphous metallic materials. Adv. Mater. **26**: 5518–5524. DOI: 10.1002/adma.201401595.
81. Wu, G., Chan, K.-C., Zhu, L., et al. (2017). Dual-phase nanostructuring as a route to high-strength magnesium alloys. Nature **545**: 80–83. DOI: 10.1038/nature21691.
82. Zhu, J., Hu, Z., Guo, S., et al. (2023). Non-epitaxial growth of highly oriented transition metal dichalcogenides with density-controlled twin boundaries. The Innovation **4**: 100502. DOI: 10.1016/j.xinn.2023.100502.
83. Zhao, W., Yan, Y., Chen, X., et al. (2022). Combining printing and nanoparticle assembly: Methodology and application of nanoparticle patterning. The Innovation **3**: 100253. DOI: 10.1016/j.xinn.2022.100253.
84. Li, S., Dong, M., Peng, M., et al. (2022). Crystal-phase engineering of pdcu nanoalloys facilitates selective hydrodeoxygenation at room temperature. The Innovation **3**: 100189. DOI: 10.1016/j.xinn.2021.100189.
85. Wuttig, M. and Yamada, N. (2007). Phase-change materials for rewriteable data storage. Nat. Mater. **6**: 824–832. DOI: 10.1038/nmat2009.
86. Wöltgens, H.W. (2003). Combinatorial material synthesis applied to Ge-Sb-Te based phase change materials. PhD thesis (RWTH Aachen University).
87. Wang, W.H. (2009). Bulk metallic glasses with functional physical properties. Adv. Mater. **21**: 4524–4544. DOI: 10.1002/adma.200901053.
88. Wang, W.H., Dong, C., and Shek, C.H. (2004). Bulk metallic glasses. Mat. Sci. Eng. R. **44**: 45–89. DOI: 10.1016/j.mser.2004.03.001.
89. Torquato, S. (2000). Hard knock for thermodynamics. Nature **405**: 521–523. DOI: 10.1038/35014711.

FUNDING AND ACKNOWLEDGMENTS

This work was supported by the Shenzhen Basic Research Fund (Grant No. JCYJ20220818100612027). We would also like to acknowledge the Major Science and Technology Infrastructure Project of Material Genome Big-science Facilities Platform supported by Municipal Development and Reform Commission of Shenzhen. The funders had no role in study design, data collection and analysis, decision to publish or preparation of the manuscript.

AUTHOR CONTRIBUTIONS

The manuscript was co-authored by all the authors. X.-D. Xiang conceived and directed the project. X.-D. Xiang and Hao-De Dong collected, processed the data and performed analysis. Zi-Kui Liu and Hong Wang made important contributions on scientific concepts, discussions and suggestions. Peng Zhang, Ming-Yang Qin and Jian Hui assisted with the data analysis and discussions to improve the manuscript.

DECLARATION OF INTERESTS

The authors declare no competing interests.

DATA AND CODE AVAILABILITY

The authors state that the primary data supporting the findings of this study are presented within the paper. Additional data are available upon reasonable request from the corresponding author.

LEAD CONTACT WEBSITE

https://www.sustech.edu.cn/en/faculties/xiangxiaodong.html